

Efficient Ruddlesden–Popper Perovskite Light-Emitting Diodes with Randomly Oriented Nanocrystals

Hyeon-Dong Lee, Hobeom Kim, Himchan Cho, Wonhee Cha, Yongseok Hong, Young-Hoon Kim, Aditya Sadhanala, Vijay Venugopalan, Joo Sung Kim, Jin Woo Choi, Chang-Lyoul Lee, Dongho Kim, Hoichang Yang, Richard H. Friend, and Tae-Woo Lee*

Ruddlesden–Popper phase (RP-phase) perovskites that consist of 2D perovskite slabs interleaved with bulky organic ammonium (OA) are favorable for light-emitting diodes (LEDs). The critical limitation of LED applications is that the insulating OA arranged in a preferred orientation limits charge transport. Therefore, the ideal solution is to achieve a randomly connected structure that can improve charge transport without hampering the confinement of the electron–hole pair. Here, a structurally modulated RP-phase metal halide perovskite (MHP), $(\text{PEA})_2(\text{CH}_3\text{NH}_3)_{m-1}\text{Pb}_m\text{Br}_{3m+1}$ is introduced to make the randomly oriented RP-phase unit and ensure good connection between them by applying modified nanocrystal pinning, which leads to an increase in the efficiency of perovskite LEDs (PeLEDs). The randomly connected RP-phase MHP forces contact between inorganic layers and thereby yields efficient charge transport and radiative recombination. Combined with an optimal dimensionality, $(\text{PEA})_2(\text{CH}_3\text{NH}_3)_2\text{Pb}_3\text{Br}_{10}$, the structurally modulated RP-phase MHP exhibits increased photoluminescence quantum efficiency, from 0.35% to 30.3%, and their PeLEDs show a 2,018 times higher current efficiency (20.18 cd A^{-1}) than in the 2D PeLED (0.01 cd A^{-1}) and 673 times than in the 3D PeLED (0.03 cd A^{-1}) using the same film formation process. This approach provides insight on how to solve the limitation of RP-phase MHP for efficient PeLEDs.

diodes (LEDs).^[1–9] MHPs have great potential to replace the currently used light emitters such as organic emitters (e.g., Ir(ppy)₃) and II–VI, III–V, IV–VI semiconducting quantum dots (QDs, e.g., CdSe/ZnS QDs), because of 1) excellent optical and electronic properties (e.g., high photoluminescence quantum efficiency, PLQE, high charge-carrier mobility, narrow emission spectrum (full-width at half-maximum $\leq 20 \text{ nm}^{[10]}$) and 2) easy color tunability by control of composition, solution processability, and low material cost, which are suitable traits for commercialization. The record efficiency of perovskite LEDs (PeLEDs) has been updated frequently. For visible-emitting PeLEDs, the initial external quantum efficiencies (EQE) were 0.1% and 0.125% in 2014,^[10,11] 8.53% in late 2015,^[1] 9.3% in early 2017,^[12] 14.36% in early 2018,^[4] and 21.3% in late 2018.^[13]

Ruddlesden–Popper (RP) phase is a multilayered structure of MHP; the chemical formula is $\text{A}'_2\text{A}_{n-1}\text{B}_n\text{X}_{3n+1}$, where A and A' are organic ammonium cations (e.g., methylammonium MA⁺ and phenylethylammonium PEA⁺) or alkali metal cations (generally, Cs⁺), B is a transition metal cation (generally, Pb²⁺), and X is a halide anion (I⁻, Br⁻, Cl⁻).^[5,14] The A'-site cations are

1. Introduction

Metal halide perovskites (MHPs) have recently received enormous attention from researchers in the field of light-emitting

and A' are organic ammonium cations (e.g., methylammonium MA⁺ and phenylethylammonium PEA⁺) or alkali metal cations (generally, Cs⁺), B is a transition metal cation (generally, Pb²⁺), and X is a halide anion (I⁻, Br⁻, Cl⁻).^[5,14] The A'-site cations are


H.-D. Lee, Dr. H. Kim, Dr. H. Cho, Dr. Y.-H. Kim, J. S. Kim
Department of Materials Science and Engineering
Seoul National University
1 Gwanak-ro, Gwanak-gu, Seoul 08826, Republic of Korea

W. Cha, Y. Hong, Prof. D. Kim
Department of Chemistry
Yonsei University
50 Yonsei-ro Seodaemun-gu, Seoul 03722, Republic of Korea
Dr. A. Sadhanala, Dr. V. Venugopalan, Prof. R. H. Friend
Cavendish Laboratory
University of Cambridge
19 J J Thomson Avenue, Cambridge CB3 0HE, UK

Dr. J. W. Choi, Dr. C.-L. Lee
Advanced Photonics Research Institute (APRI)
Gwangju Institute of Science and Technology (GIST)
123 Cheomdangwagi-ro, Buk-gu, Gwangju 61005, Korea

Prof. H. Yang
Department of Chemical Engineering
Inha University
100 Inha-ro, Incheon 22212, Republic of Korea

Prof. T.-W. Lee
Department of Materials Science and Engineering
Nano Systems Institute (NSI)
Institute of Engineering Research
Research Institute of Advanced Materials
BK21 PLUS SNU Materials Division for Educating Creative Global Leaders
Seoul National University
1 Gwanak-ro Gwanak-gu, Seoul 08826, Republic of Korea
E-mail: twlees@snu.ac.kr

 The ORCID identification number(s) for the author(s) of this article can be found under <https://doi.org/10.1002/adfm.201901225>.

DOI: 10.1002/adfm.201901225

larger than A-site cations, and intercalate between 2D MHP sheets; the number n of inorganic planes in the 2D MHP sheets determines the dimensionality of RP-phase MHPs. The energy level and bandgap of RP-phase MHPs depend on the dimensionality; because of the quantum confinement effect, the bandgap gradually increases as n decreases from ∞ (3D) to 1 (2D). Compared with 3D MHP polycrystalline films (ABX₃), RP-phase MHP polycrystalline films have stronger electron-hole pairs confinement, more uniform film morphology with smaller grains and superior stability under exposure to light and moisture.^[15,16] Because of these advantages over 3D MHPs, RP-phase MHPs are often used in PeLEDs. The first RP-phase MHPs emitter was demonstrated by controlling the ratio of MA to PEA, and their PeLEDs showed low efficiency in green color (4.90 cd A⁻¹, 2935 cd m⁻²).^[14] The RP-phase PeLED with (PEA)₂(MA)₄Pb₅Br₁₆ exhibits a high EQE of 7.4% in green color and a systematic analysis for a cascade energy transfer (or energy funneling effect) was reported.^[17] Control of the ratio of PEA to MA in RP-phase MHP drives a cascade energy transfer (or energy funneling effect) that induces carrier localization, and yields PEA₂(MA) _{$n-1$} Pb _{n} I _{$3n+1$} near-infrared PeLEDs with EQE = 8.8%.^[18] Tuning the ratio of 1-naphthylmethylamine iodide (NFPI₇):FAI:PbI₂ widens the quantum well of RP-phase MHP and thereby reduces nonradiative Auger recombination and alleviates efficiency roll-off; as a result, RP-phase PeLEDs have achieved EQE = 12.7%.^[19] Phase engineering of RP-phase MHP and surface passivation by trioctylphosphine oxide treatment yielded a PeLED with maximum EQE = 14.36%.^[4]

In terms of the electron-hole pairs confinement, RP-phase MHPs of $n = 1$ or 2 can be more desirable for PeLEDs. However, when the proportion of A'-site cation is higher (e.g., 100% for $n = 1$ and 67% for $n = 2$) than that of A-site cation, charge transport in RP-phase MHP layers is severely hindered by bulky A'-site cations, so the efficiency of radiative recombination in PeLEDs is reduced. Directional growth of RP-phase MHPs causes a formation of an insulating organic layer, which further hinders charge transport. During spin-coating, RP-phase MHP crystals grow in a preferential orientation, which is most likely parallel to the substrate, and consequently form multilayered RP-phase nanoplatelets with intercalating A'-site cations that impede charge transport.^[20] Therefore, an increase in EQE of PeLEDs requires the development of both an optimal nanostructure of RP-phase MHP films which allows high PLQE and high charge transport ability, and a process to fabricate RP-phase MHP films that have the optimal nanostructure.

Here, we demonstrate the high-efficiency RP-phase PeLEDs by overcoming limited charge transport in PeLEDs. This ability was increased by controlling the crystallization of MHP grains to yield an optimal grain-packing structure that consists of randomly oriented isotropic nanocrystals instead of aligned anisotropic nanoplatelets. Furthermore, control of the dimensionality of MHP crystals increased the PLQE of MHP films from 0.35% to 30.3%. These approaches led to high electroluminescence (EL) efficiency of 20.18 cd A⁻¹, which is 2018 times higher than in the 2D PeLED control device (0.01 cd A⁻¹) and 673 times than in the 3D PeLED (0.03 cd A⁻¹) based on the same processes.

2. Results and Discussion

RP-phase MHP films with different dimensionalities were fabricated by spin-coating the following MHP precursor solutions: MAPbBr₃ (3D structure), PEA₂PbBr₄ (2D structure), and (PEA)₂(MA) _{$m-1$} Pb _{m} Br _{$3m+1$} ($m = 2-5$) (quasi-2D structure; RP-phase) dissolved in dimethyl sulfoxide (DMSO; Table S1, Supporting Information). The average n ($\langle n \rangle$) in RP-phase MHP film increases with increase in m in the precursor solution, although the relationship is not direct. RP-phase MHP films consist of ensembles of RP-phase crystals with different n , so we assigned sample codes $\langle n \rangle = 1-5$ and $\langle n \rangle = \infty$, respectively, to RP-phase MHP films fabricated from precursor solutions (PEA)₂(MA) _{$m-1$} Pb _{m} Br _{$3m+1$} ($m = 1-5, \infty$) (Table S1, Supporting Information).

To increase the charge transport ability of RP-phase MHP film, its nanostructure was altered by using an optimized nanocrystal pinning (NCP) process which incorporates a non-volatile solvent (toluene) unlike the conventional NCP (chloroform solvent) that manipulates the shape and orientation of MHP crystals by inducing immediate crystallization.^[1,21] Twelve RP-phase MHP films were prepared (Figure S1a,b, Supporting Information) that had different combinations of $\langle n \rangle$ (1-5, ∞) with and without NCP. We hypothesized that RP-phase MHP films that were prepared using NCP would consist of MHP crystals with random orientation, rounder shape, and smaller $\langle n \rangle$ compared with those of films without NCP (Figure 1). When the MHP precursor solution is spin-coated without NCP, MHP crystals grow in in-plane directions (i.e., parallel to the substrate) (Figure S1c, Supporting Information).^[20] In the intermediate phase during spin-coating, RP-phase MHP nanoparticles surrounded by DMSO molecules form stacks on the (001) plane of PbBr₆ layers. As DMSO evaporates slowly, large PEA⁺ adheres preferentially to the (001) plane of PbBr₆ by strong Van der Waals force, and the growth of crystals can occur mostly in in-plane directions.^[22] Therefore, RP-phase MHP crystals with a quasi-2D planar structure form. In contrast, when NCP is applied to the spinning precursor solution of the intermediate

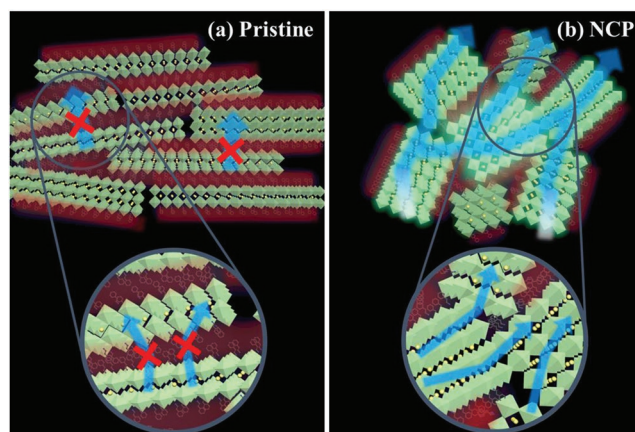


Figure 1. Schematic illustrations of mixed PEA₂MA _{$m-1$} Pb _{m} Br _{$3m+1$} perovskite. a) Without NCP, RP-phase perovskite with plate-like structure has preferential orientation. b) With NCP, RP-phase perovskite with particle-like structure has random orientation. Blue arrows indicate the charge-transport process in RP-phase MHP emitter.

phase, the DMSO molecules that are attached to the (001) plane are instantaneously replaced with toluene molecules that do not dissolve MHPs, then the crystallization occurs very rapidly without any preferential in-plane growth. Therefore, the formed RP-phase MHP crystals have a random orientation. This type of structurally modulated nanostructure can be effective to facilitate charge transport in PeLEDs by increasing the change of contact between adjacent MHP crystals (Figure 1).

The crystal structure of RP-phase MHP films was determined by analyzing grazing-incidence X-ray diffraction (GIXD) patterns (Figure 2 and Figures S8 and S9, Supporting Information). Without any NCP process, a 3D film with $\langle n \rangle = \infty$ had

highly ordered crystals, where (001) planes were highly oriented parallel to the film surface, as determined by spot-like X-ray reflections along both Q_z (out-of-plane or surface normal) and Q_x (in-plane or surface parallel) axes, respectively (Figure S8f, Supporting Information). In contrast, an NCP-treated 3D film showed randomly oriented X-ray reflections of (001), (110), (002), (210), and (112) crystal planes at Q values of approximately 1.065, 1.508, 2.110, 2.346, and 2.555 \AA^{-1} , respectively (Figure S8l, Supporting Information). RP-phase MHP films with $\langle n \rangle = 2-5$ showed a typical phase transition from 3D to 2D with a decrease in $\langle n \rangle$ (i.e., an increase of PEA⁺ proportion).^[14] These films had highly ordered crystal structures including 3D,

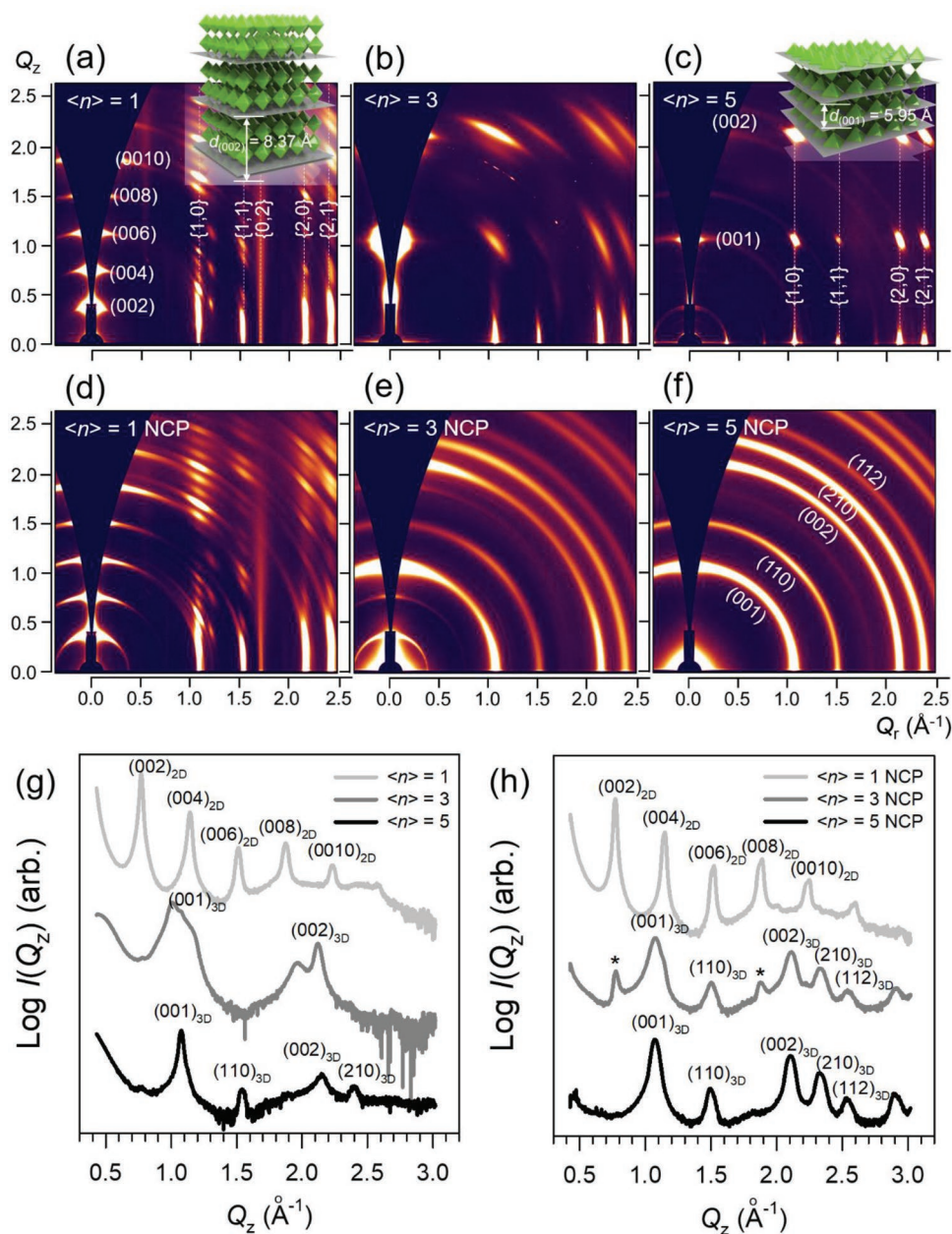


Figure 2. a–f) 2D GIXD patterns of mixed $\text{PEA}_2\text{MA}_{m-1}\text{Pb}_m\text{Br}_{3m+1}$ perovskite films with $\langle n \rangle = 1, 3$, and 5 , a–c) before and d–f) after NCP process. g,h) 1D out-of-plane X-ray profiles extracted from the corresponding GIXD patterns: g) pristine, h) NCP-treated films (after NCP, RP-phase perovskite crystals were randomly oriented).

quasi-2D, and 2D layers with a similar in-plane structure but vertically distinguishable domain spacing (referred to as $d_{(001)2D}$ or $d_{(001)3D}$) values ranging from 5.950 (for a 3D-like crystal) to 16.74 Å (for a 2D-like crystal), depending on the proportion of large PEA⁺ intercalated between PbBr₆ layers, indicating that the RP-phase MHP crystals spontaneously grew along the in-plane direction in the films due to the influence of PEA⁺ cations. As the proportion of PEA⁺ increased, the films had the 2D crystal phases including multiple-stacked PbBr₆ layers vertically separated by PEA⁺ cations, similar to the PEA₂PbBr₄ film with $\langle n \rangle = 1$ showing highly ordered (00 l) crystal planes along the Q_z axis.^[23] It is found that the existence of PEA⁺ cations hinders the formation of 3D-like RP-phase crystals, and does not disturb a crystal growth along in-plane directions.

NCP process substantially changed the crystal structure of all the RP-phase MHP films, specifically, with $\langle n \rangle = 2$ –5 and $\langle n \rangle = \infty$. The 2D GIXD patterns of films with $\langle n \rangle = 3$ and 5 showed (001), (110), (002), (210), and (112) reflections indicated in the 3D MAPbBr₃ film including randomly oriented crystals, as determined by the Debye rings in 2D GIXD pattern (Figure 2e,f and Figure S8, Supporting Information). These changes in 2D GIXD patterns support our hypothesis that the use of NCP inhibits spontaneous growth of RP MHP along in-plane directions. NCP also affected the crystal orientation of RP-phase MHP (Figure 2c–h). NCP changes the packing structure of RP-phase MHP crystals from aligned platelets to disordered crystallites by fast solvent evaporation, before MHP crystals can grow layer by layer.

The optical properties (i.e., steady-state PL, PL lifetime, PLQE, steady-state/transient absorption, TA) of RP-phase MHP films were correlated with their nanostructures. As $\langle n \rangle$ decreased from ∞ to 1, additional peaks at shorter wavelength emerged in PL and absorption spectra (Figure 3a–d). In absorption spectra, upon addition of PEA, the additional peaks at 401, 434, and 450 nm were observed, which were induced by the newly appearing domain, and these peaks were assigned to crystals that had $n = 1, 2, 3$, respectively (Figure 3c,d); the corresponding PL peaks occurred at 409, 436, and 476 nm (Figure 3a,b and Figure S2, Supporting Information). The peaks at the range of 511–530 nm of $\langle n \rangle = 2$ –5 originated from MHP crystals that had $n \geq 4$. As $\langle n \rangle$ decreased from ∞ to 3, the PL peak showed a gradual blue-shift (Figure 3a,b and Figure S7, Supporting Information) and PLQE significantly increased (0.02% at $\langle n \rangle = \infty$ and 4.0% at $\langle n \rangle = 3$) (Figure 3e,f) due to the quantum confinement effect.^[24–26] However, although the MHP crystals with low n (e.g., $n = 1, 2$) have a quantum confinement effect, the PLQE steeply decreased as $\langle n \rangle$ further decreased from 3 to 1 (0.03% at $\langle n \rangle = 1$); this change may be a result of fast electron–hole pairs quenching rates at room temperature in MHP crystals as n decreases.^[27–29]

Use of NCP altered the optical properties of RP-phase MHP films as well as structural properties. The intensities of the appeared absorption peaks (at 401, 434, and 450 nm) greatly decreased in the film that had $\langle n \rangle = 2$ and the peaks became almost negligible at the film of $\langle n \rangle = 3$ (Figure 3c,d). This result is in agreement with the observation in X-ray diffraction (XRD) that NCP decreased the intensities of the diffraction peaks of 2D PEA₂PbBr₄ (Figure 2a,b and Figure S8, Supporting Information).

Change in $\langle n \rangle$ caused a blue-shift in the PL peak positions, and NCP also affected this shift. In films that had $\langle n \rangle = 1$

and ∞ , there is no difference in PL peaks according to NCP method. However, after NCP, the PL peak of the film with $\langle n \rangle = 3$ shifted from 527 to 520 nm due to the quantum confinement effect (Figure S4c, Supporting Information). Also, at $\langle n \rangle = 2$ the blue-shift was 19 nm in the film prepared without NCP, and 11 nm in the film prepared with NCP. The different blue-shift occurs because \bar{n} increased in the films prepared using NCP, and this increase of \bar{n} weakens the quantum confinement compared to films without NCP.

Furthermore, NCP increased the PL intensity (Figure S4, Supporting Information) and PLQE (Figure 3e,f) of RP-phase MHP films ($\langle n \rangle = 1$ –5); most strikingly, in films of $\langle n \rangle = 3$, NCP increased the PLQE from 4.0% to 30.3%. This increase was caused by the formation of uniform films and reduction of grain size (Figure S10, Supporting Information). Small grain size can induce strong radiative recombination process, which can improve PLQE and EQE of LED device.^[1,5,21,25,30,31] The film with 3D MHP had low PLQE due to the poor surface coverage and the weak spatial confinement of electron–hole pair in large grain >100 nm at room temperature (Figure S11f, Supporting Information). Despite the strong quantum confinement, 2D MHP film also had low PLQE because the electron–hole pair can be quenched through nonradiative recombination process caused by trap states.^[27–29] By controlling the ratio of PEA to MA in RP-phase MHP, we obtained full surface coverage and grain size of 30.4 nm with strongly enhanced PLQE (Figure S11, Supporting Information). This result showed 87 times higher PLQE (30.3%) than in the 2D PeLED (0.35%).

Time-correlated single-photon counting (TCSPC) analysis was conducted to identify changes in PL lifetime according to the NCP treatment. NCP treatment increased PL lifetime (Figure 3h). As the value of $\langle n \rangle$ changed from $\langle n \rangle = 2, 4$ to $\langle n \rangle = 3$, the electron–hole pair confinement was enhanced due to the reduction of grain size, so PL lifetime increased from 23.9, 28.5 to 34.4 ns. RP-phase MHP with $\langle n \rangle = 3$ had dominantly excitonic recombination process rather than bimolecular recombination process.^[31] The observed increase in PL lifetime is in good agreement with previous results that RP-phase MHP with $\langle n \rangle = 3$ has the smallest grain size and highest PLQE. Furthermore, in the case of RP-phase MHP with $\langle n \rangle = 3$, NCP increased PL lifetime from 34.3 to 47.0 ns due to the more radiative recombination process (Figure 3h).

We have carried out TA spectroscopy measurement to investigate the dynamics of the carriers in structurally modulated RP-phase perovskites, which allows us to understand the energy transfer dynamics of photoexcited carriers. The TA results support that the NCP hampered the formation of 2D-like RP-phase MHP ($n = 1$ –3) in which fast electron–hole pairs quenching is favored and promotes the formation of 3D-like RP-phase MHP crystals ($n \geq 4$) in which radiative recombination is favored. As shown in Figure 4, the dominant bleach peak was observed at 400 nm in 2D MHP, and at 525 nm in 3D MHP (Figure 4a,d). In the case of RP-phase MHP which has multiple layers with different bandgaps, distinctive bleach peaks were observed in the TA spectrum of the RP-phase MHP with $\langle n \rangle = 3$ (Figure 4b,f and Figure S13, Supporting Information). In the case of MHP film with $\langle n \rangle = 2$, these distinctive peaks became stronger; this change suggests that multiple layers composed of 2D-like RP-phase MHP ($n = 1$ –3) were formed

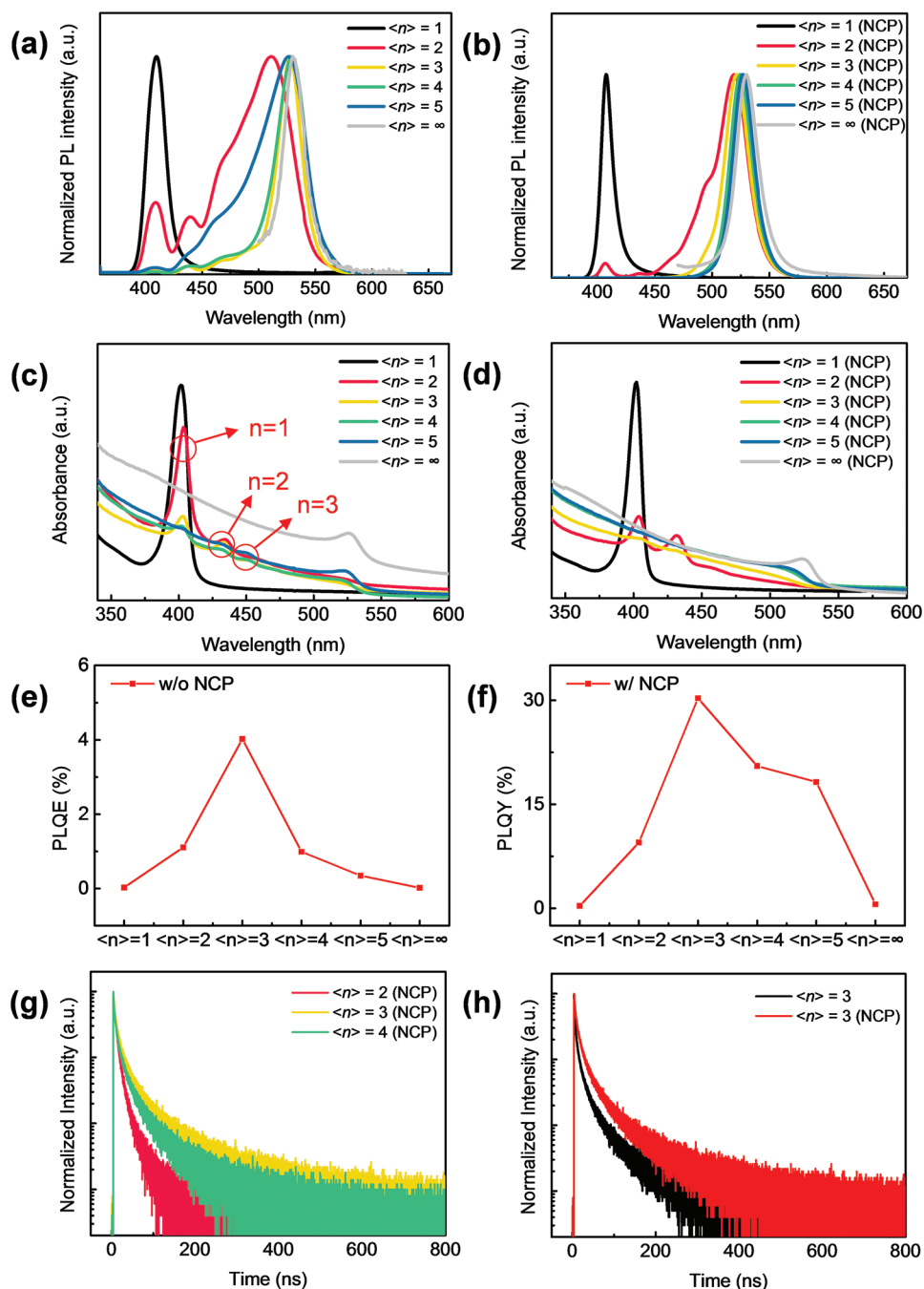


Figure 3. a,b) UV-vis absorption spectra of mixed $\text{PEA}_2\text{MA}_{m-1}\text{Pb}_m\text{Br}_{3m+1}$ perovskite films a) without and b) with NCP in samples from $\langle n \rangle = 1$ to $\langle n \rangle = \infty$. NCP weakened the intensity of the peak that corresponds to low-number layers. c,d) PL spectra of mixed $\text{PEA}_2\text{MA}_{m-1}\text{Pb}_m\text{Br}_{3m+1}$ perovskite films c) without and d) with NCP in samples from $\langle n \rangle = 1$ to $\langle n \rangle = \infty$. NCP sharpened the peaks. e,f) PLQY of mixed $\text{PEA}_2\text{MA}_{m-1}\text{Pb}_m\text{Br}_{3m+1}$ perovskite films e) without and f) with NCP from $\langle n \rangle = 1$ to $\langle n \rangle = \infty$. g) TCSPC data of mixed $\text{PEA}_2\text{MA}_{m-1}\text{Pb}_m\text{Br}_{3m+1}$ perovskite films in the NCP process samples from $\langle n \rangle = 2$ to $\langle n \rangle = 4$ and h) with and without NCP.

(Figures S1c, S13h, and S14h, Supporting Information). These 2D-like RP-phase MHP layers can limit the carrier transport in vertical devices. On the other hand, with NCP treatment, the TA spectrum of structure-modulated RP-phase MHP only has a bleach peak, i.e., the 2D-like MHP layers disappeared (Figure 4c,g and Figure S14, Supporting Information). These results are in good agreement with the steady-state absorption

spectra, which suggested that structure-modulated RP-phase MHP acts like a single phase rather than a mixture of domains with different bandgap energy. This change of TA spectrum is originated from the structure modulation that yielded randomly orientated isotropic RP-phase MHP nanocrystals (Figure 4g).

TA dynamics suggested that excited charges were funneled into the lowest-bandgap state in a short time, which can

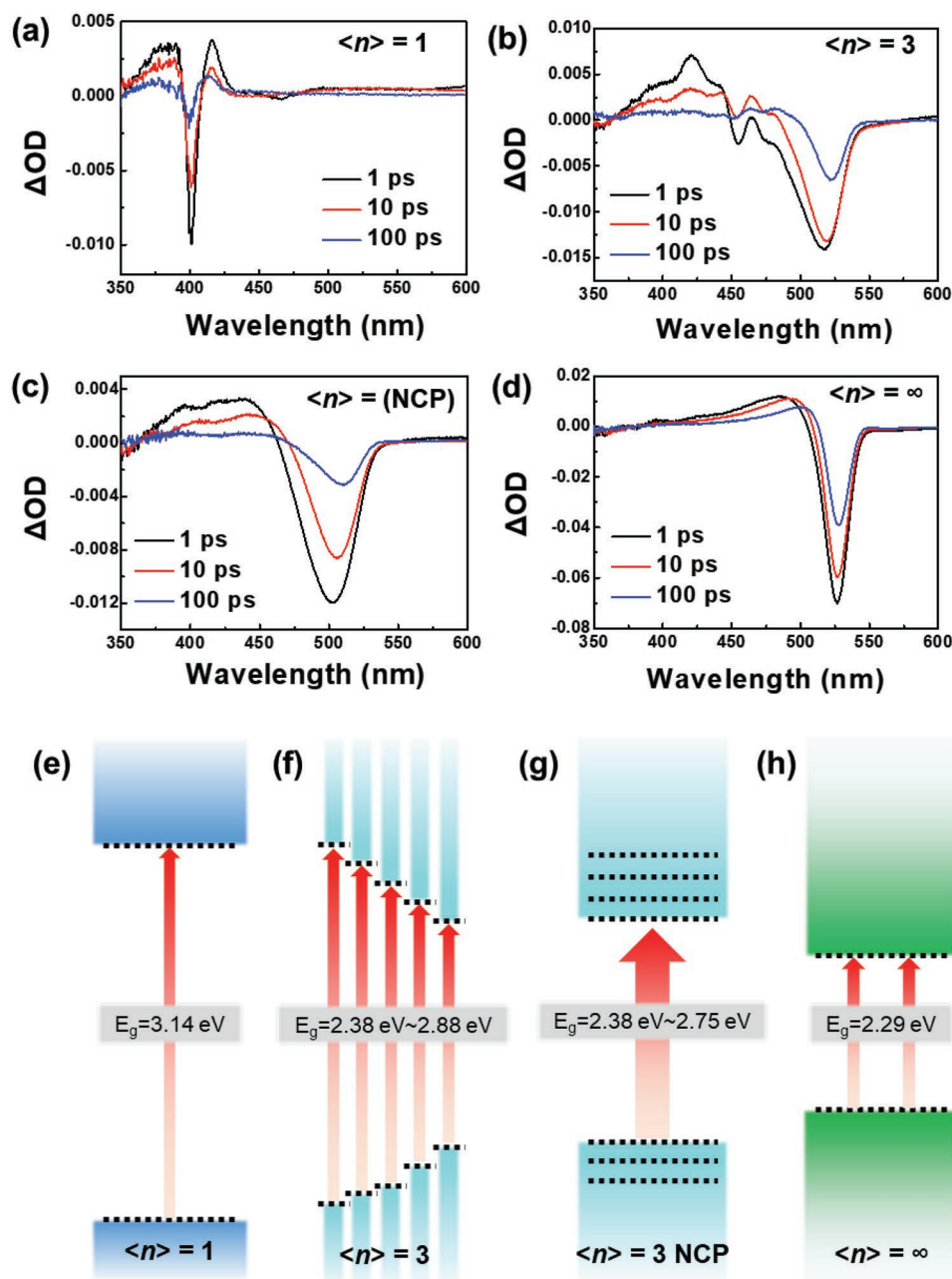


Figure 4. TA spectra of mixed $\text{PEA}_2\text{MA}_{m-1}\text{Pb}_m\text{Br}_{3m+1}$ perovskite films of a) $\langle n \rangle = 1$, b) $\langle n \rangle = 3$, c) $\langle n \rangle = 3$ with NCP, and d) $\langle n \rangle = \infty$. Schematic diagram of mixed $\text{PEA}_2\text{MA}_{m-1}\text{Pb}_m\text{Br}_{3m+1}$ perovskite films of e) $\langle n \rangle = 1$, f) $\langle n \rangle = 3$, g) $\langle n \rangle = 3$ with NCP, and h) $\langle n \rangle = \infty$. In RP-phase perovskite ($\langle n \rangle = 3$), the peak that corresponds to the lower layer is observed before NCP, but not after NCP; this change suggests that the specific layer disappears and forms a particle-like structure.

induce strong radiative recombination process (Figure S15, Supporting Information). The excited charges were cascaded from higher-bandgap states to the lowest-bandgap state in 100 fs to 1 ps timescales, and the funneling process was substantially complete within 100 ps. These funneling processes maximize the radiative recombination process by accumulating charge to the lowest-band state before nonradiative recombination process occurs, thereby increasing the efficiency of RP-phase PeLEDs.

3. Conclusion

In conclusion, we achieved an RP-phase MHP emitter with a randomly oriented and connected structure by using modified NCP using toluene. NCP modulates the structure of RP-phase MHP, so the carriers are effectively transported through the connected interface between the inorganic layers and the current density in PeLEDs is increased, thus improving the efficiency of the RP-phase PeLEDs. NCP greatly increased the efficiency

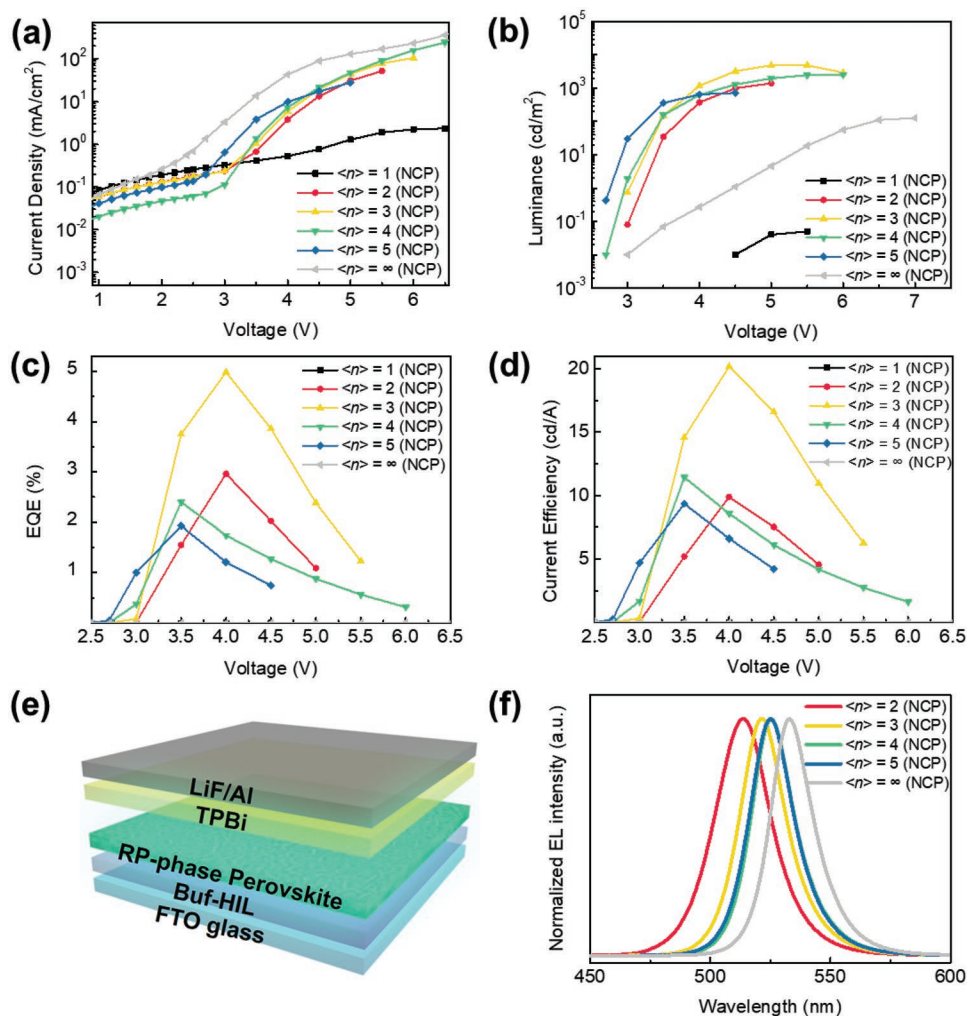


Figure 5. Luminescence parameters of mixed $\text{PEA}_2\text{MA}_{m-1}\text{Pb}_m\text{Br}_{3m+1}$ perovskite with fluorine doped tin oxide (FTO)/Buf-HIL/perovskite film/TPBi (50 nm)/LiF (1 nm)/Al (100 nm) structure: a) J - V - L curve of the device with mixed $\text{PEA}_2\text{MA}_{m-1}\text{Pb}_m\text{Br}_{3m+1}$ perovskite with NCP; c) external quantum efficiency–voltage curve of the device with mixed $\text{PEA}_2\text{MA}_{m-1}\text{Pb}_m\text{Br}_{3m+1}$ perovskite with NCP; d) current efficiency–voltage curve of the device with mixed $\text{PEA}_2\text{MA}_{m-1}\text{Pb}_m\text{Br}_{3m+1}$ perovskite with NCP; b) schematic illustration of device structure. e) Schematic illustration of device structure. f) EL peaks blue-shifted as an amount of PEA increased.

of RP-phase PeLEDs (Figure 5 and Figures S16 and S17, Supporting Information). The PeLEDs with 3D MHP emitter showed low device efficiency of PeLED (0.03 cd A^{-1} at $\langle n \rangle = \infty$) due to the poor surface coverage and the large grain size. PeLED with 2D MHP emitter also showed poor device efficiency (0.01 cd A^{-1} at $\langle n \rangle = 1$) due to the nonradiative recombination process caused by trap states. We developed high-efficiency RP-phase PeLEDs with the maximum current efficiency of 20.18 cd A^{-1} and maximum EQE of 4.98% by applying NCP to RP-phase MHP with $\langle n \rangle = 3$. The operational lifetimes of RP-phase PeLEDs were measured by the time taken for the luminance to decrease from the initial luminance L_0 to 50%. The lifetime of RP-phase PeLEDs using $\text{PEA}_2\text{MA}_2\text{Pb}_3\text{Br}_{10}$ was improved from $L_{50} \approx 130 \text{ s}$ without NCP to $L_{50} \approx 470 \text{ s}$ with NCP at 100 cd m^{-2} (Figure S18, Supporting Information). The changes in the XRD and GIXD patterns demonstrate that the RP-phase perovskite changes the crystal orientation of the RP-phase from the preferential orientation to the random orientation according to NCP,

which is a structure that improves charge transport in the vertical devices based on RP-phase. As more PEA was added, the PL and EL spectra were blue-shifted. The luminous intensity increased with the increase of operating voltages, while the peak shift did not occur (Figure S19, Supporting Information). At the optimum composition ($\langle n \rangle = 3$ RP-phase MHPs), the highest PLQE (30.3%) was achieved due to the electron–hole pairs confinement effect. The gradual change in absorption and TA spectra supported that structurally modulated RP-phase MHPs were composed of RP structure with the random orientation that has strong radiative recombination process and good charge transport capability.

Our research suggests that the fabrication of structurally modulated RP-phase PeLEDs is a simple and effective strategy to improve the PLQE and EL efficiency of RP-phase PeLEDs. Although structurally modulated RP-phase PeLEDs have lower efficiency than state-of-the-art PR-phase PeLEDs, this approach is conceptually new in the field of conventional RP-phase

MHP research and is a major advance in the development of RP-phase PeLEDs.

4. Experimental Section

Solution Preparation: PEA and MA were purchased from GreatCell Solar. PbBr₂ was purchased from Sigma-Aldrich. All solutions had a concentration of 15 wt% in DMSO. The solution of MAPbBr₃ was mixed PbBr₂ and MABr in ratio of 1:1 (mol:mol). The solution of PEA₂PbBr₄ was mixed PbBr₂ and PEABr in ratio of 1:2 (mol:mol). The solution of RP-phase MHP was mixed PbBr₂, MABr, and PEABr in ratios of 2:1:2, 3:2:2, 4:3:2, and 5:4:2 (mol:mol) (Table S1, Supporting Information).

Device Fabrication: Substrates coated with fluorine tin oxide were sonicated sequentially in acetone and isopropyl alcohol (IPA) for 15 min each, then boiled for 15 min in IPA. The substrate was treated with ultraviolet ozone for 15 min, then a self-organized buffer HIL (Buf-HIL) was spin-coated as described previously.^[10] The precursor solution was coated onto the Buf-HIL in two steps of 500 rpm for 5 s and 3000 rpm for 60 s, respectively (conventional method). To achieve structurally modulated RP-phase perovskite, toluene solvent was put onto the perovskite film during the second spin step (NCP method). Then, the substrates were annealed on a hot plate at 90 °C for 10 min. All processes of spin-coating of MHP and encapsulation were performed in N₂ atmosphere. After transferring to the thermal evaporator under high vacuum (<10⁻⁷ Torr), 2,2',2''-(1,3,5-benzinetriyl)-tris (1-phenyl-1H-benzimidazole) (TPBi) (50 nm), LiF (1 nm), and Al (100 nm) were sequentially deposited onto the perovskite films.

Characterization and Measurement: Steady-State PL Measurement: Steady-state PL spectra of the thin film samples (glass/Buf-HIL/RP-phase MHP) were measured using a spectrofluorometer (JASCO FP-8500) without encapsulation; excitation wavelength was 280 nm (Xenon arc lamp; power = 150 W).

GIXD Measurement: GIXD measurement was conducted at beamlines 6D and 9A at the Pohang Accelerator Laboratory (PAL), Korea.^[32] MHP films were spin-coated on a Buf-HIL-coated Si wafer. An X-ray with $\lambda = 0.62382 \text{ \AA}$ and an incidence angle = 0.1°–0.2° were used in this study.

TCSPC Measurement: PL decay of the thin film samples (glass/Buf-HIL/RP-phase MHP) was measured using a TCSPC system (FluoTime, PicoQuant). The excitation wavelength of picosecond laser was 405 nm.

PeLED Characterization: The current–voltage–luminance characteristics were measured using a source-measurement (Keithley 236) and a spectroradiometer (Minolta CS2000).

PLQE Measurement: PLQE of the thin film samples (glass/Buf-HIL/RP-phase MHP) was measured using an integrating sphere method. The excitation source was a laser diode with wavelength of 405 nm and power density of 900 mW cm⁻².^[33]

TA Spectroscopy Analysis: A femtosecond time-resolved TA spectrometer used for this study was consisted of a femtosecond optical parametric amplifier (OPA, Quantronix, Palitra-FS) pumped by a Ti:sapphire regenerative amplifier system (Quantronix, Integra-C) operating at 1 kHz repetition rate and an accompanying optical detection system. The generated OPA pulses had a pulse width of ≈100 fs and an average power of 1 mW in the range 550–690 nm, which were used as pump pulses. White light continuum (WLC) probe pulses were generated using a calcium fluoride (CaF₂) window by focusing on small portion of the fundamental 800 nm pulses, which were picked off by a quartz plate before entering into the OPA. The time delay between pump and probe beams was carefully controlled by making the pump beam travel along a variable optical delay (Newport, ILS250). Intensities of the spectrally dispersed WLC probe pulses were monitored by high speed spectrometer (Ultrafast Systems). To obtain the time-resolved TA difference signal (ΔA) at a specific time, the pump pulses were chopped at 500 Hz and absorption spectra intensities were saved alternately with or without pump pulse.

Supporting Information

Supporting Information is available from the Wiley Online Library or from the author.

Acknowledgements

H.-D.L., H.K., and H.C. contributed equally to this work. This work was supported by the National Research Foundation of Korea (NRF) grant funded by the Korea government (Ministry of Science and ICT) (NRF-2016R1A3B1908431). H.Y. acknowledges the grant provided by the National Research Foundation of Korea (NRF2017R1A2B4009313).

Conflict of Interest

The authors declare no conflict of interest.

Keywords

carrier transport, nanocrystal orientation, nanocrystal pinning, quasi-2D perovskite, structural modulation

Received: February 10, 2019

Revised: March 11, 2019

Published online: April 1, 2019

- [1] H. Cho, S. H. Jeong, M. H. Park, Y.-H. Kim, C. Wolf, C. L. Lee, J. H. Heo, A. Sadhanala, N. S. Myoung, S. Yoo, S. H. Im, R. H. Friend, T.-W. Lee, *Science* **2015**, *350*, 1222.
- [2] K. Lin, J. Xing, L. N. Quan, F. P. G. de Arquer, X. Gong, J. Lu, L. Xie, W. Zhao, D. Zhang, C. Yan, W. Li, X. Liu, Y. Lu, J. Kirman, E. H. Sargent, Q. Xiong, Z. Wei, *Nature* **2018**, *562*, 245.
- [3] Y. Cao, N. Wang, H. Tian, J. Guo, Y. Wei, H. Chen, Y. Miao, W. Zou, K. Pan, Y. He, H. Cao, Y. Ke, M. Xu, Y. Wang, M. Yang, K. Du, Z. Fu, D. Kong, D. Dai, Y. Jin, G. Li, H. Li, Q. Peng, J. Wang, W. Huang, *Nature* **2018**, *562*, 249.
- [4] X. Yang, X. Zhang, J. Deng, Z. Chu, Q. Jiang, J. Meng, P. Wang, L. Zhang, Z. Yin, J. You, *Nat. Commun.* **2018**, *9*, 570.
- [5] a) H. Cho, J. S. Kim, C. Wolf, Y.-H. Kim, H. J. Yun, S. H. Jeong, A. Sadhanala, V. Venugopalan, J. W. Choi, C. L. Lee, R. H. Friend, T.-W. Lee, *ACS Nano* **2018**, *12*, 2883; b) H. Cho, Y.-H. Kim, C. Wolf, H.-D. Lee, T.-W. Lee, *Adv. Mater.* **2018**, *30*, 1704587.
- [6] a) Y.-H. Kim, S. Kim, S. H. Jo, T.-W. Lee, *Small Methods* **2018**, *2*, 1800093; b) Y.-H. Kim, J. S. Kim, T.-W. Lee, *Adv. Mater.* **2018**, e1804595, <https://doi.org/10.1002/adma.201704587>; c) Y.-H. Kim, C. Wolf, H. Kim, T.-W. Lee, *Nano Energy* **2018**, *52*, 329.
- [7] T. Jeon, H. M. Jin, S. H. Lee, J. M. Lee, H. Il Park, M. K. Kim, K. J. Lee, B. Shin, S. O. Kim, *ACS Nano* **2016**, *10*, 7907.
- [8] T. Jeon, S. J. Kim, J. Yoon, H. R. Hong, T.-W. Lee, J. S. Kim, B. Shin, S. O. Kim, *Adv. Energy Mater.* **2017**, *7*, 1602596.
- [9] S. J. Kim, J. Byun, T. Jeon, H. M. Jin, H. R. Hong, S. O. Kim, *ACS Appl. Mater. Interfaces* **2018**, *10*, 2490.
- [10] Y.-H. Kim, H. Cho, J. H. Heo, T. S. Kim, N. S. Myoung, C. L. Lee, S. H. Im, T.-W. Lee, *Adv. Mater.* **2015**, *27*, 1248.
- [11] Z.-K. Tan, R. S. Moghaddam, M. L. Lai, P. Docampo, R. Higler, F. Deschler, M. Price, A. Sadhanala, L. M. Pazos, D. Credgington, F. Hanusch, T. Bein, H. J. Snaith, R. H. Friend, *Nat. Nanotechnol.* **2014**, *9*, 687.
- [12] Z. Xiao, R. A. Kerner, L. Zhao, N. L. Tran, K. M. Lee, T.-W. Koh, G. D. Scholes, B. P. Rand, *Nat. Photonics* **2017**, *11*, 108.

- [13] T. Chiba, Y. Hayashi, H. Ebe, K. Hoshi, J. Sato, S. Sato, Y. J. Pu, S. Ohisa, J. Kido, *Nat. Photonics* **2018**, 12, 681.
- [14] J. Byun, H. Cho, B. C. Wolf, M. Jang, A. Sadhanala, R. H. Friend, H. Yang, T.-W. Lee, *Adv. Mater.* **2016**, 28, 7515.
- [15] I. C. Smith, E. T. Hoke, D. Solis-Ibarra, M. D. McGehee, H. I. Karunadasa, *Angew. Chem., Int. Ed.* **2014**, 53, 11232.
- [16] L. N. Quan, M. Yuan, R. Comin, O. Voznyy, E. M. Beauregard, S. Hoogland, A. Buin, A. R. Kirmani, K. Zhao, A. Amassian, D. H. Kim, E. H. Sargent, *J. Am. Chem. Soc.* **2016**, 138, 2649.
- [17] O. M. Bakr, J. Z. Fan, O. Voznyy, M. Yuan, F. P. García de Arquer, Y. Li, Z. Lu, R. Sabatini, H. Tan, Y. Zhao, D. H. Kim, G. Walters, J. Pan, R. Comin, L. N. Quan, E. H. Sargent, *Nano Lett.* **2017**, 17, 3701.
- [18] M. Yuan, L. N. Quan, R. Comin, G. Walters, R. Sabatini, O. Voznyy, S. Hoogland, Y. Zhao, E. M. Beauregard, P. Kanjanaboos, Z. Lu, D. H. Kim, E. H. Sargent, *Nat. Nanotechnol.* **2016**, 11, 872.
- [19] W. Zou, R. Li, S. Zhang, Y. Liu, N. Wang, Y. Cao, Y. Miao, M. Xu, Q. Guo, D. Di, L. Zhang, C. Yi, F. Gao, R. H. Friend, J. Wang, W. Huang, *Nat. Commun.* **2018**, 9, 608.
- [20] D. B. Mitzi, *J. Mater. Chem.* **2004**, 14, 2355.
- [21] M.-H. Park, S.-H. Jeong, H.-K. Seo, C. Wolf, Y.-H. Kim, H. Kim, J. Byun, J. S. Kim, H. Cho, T.-W. Lee, *Nano Energy* **2017**, 42, 157.
- [22] K. Yan, M. Long, T. Zhang, Z. Wei, H. Chen, S. Yang, J. Xu, *J. Am. Chem. Soc.* **2015**, 137, 4460.
- [23] D. H. Cao, C. C. Stoumpos, O. K. Farha, J. T. Hupp, M. G. Kanatzidis, *J. Am. Chem. Soc.* **2015**, 137, 7843.
- [24] Y.-H. Kim, H. Cho, T.-W. Lee, *Proc. Natl. Acad. Sci. U. S. A.* **2016**, 113, 11694.
- [25] Y.-H. Kim, C. Wolf, Y. T. Kim, H. Cho, W. Kwon, S. Do, A. Sadhanala, C. G. Park, S. W. Rhee, S. H. Im, R. H. Friend, T.-W. Lee, *ACS Nano* **2017**, 11, 6586.
- [26] K. Zheng, Q. Zhu, M. Abdellah, M. E. Messing, W. Zhang, A. Generalov, Y. Niu, L. Ribaud, S. E. Canton, T. Pullerits, *J. Phys. Chem. Lett.* **2015**, 6, 2969.
- [27] X. Hong, T. Ishihara, A. V. Nurmikko, *Phys. Rev. B* **1992**, 45, 6961.
- [28] K. Gauthron, J. Lauret, L. Doyennette, G. Lanty, A. Al Choueiry, S. J. Zhang, L. Largeau, O. Mauguin, J. Bloch, E. Deleporte, *Opt. Express* **2010**, 18, 5912.
- [29] J.-C. Blancon, H. Tsai, W. Nie, C. C. Stoumpos, L. Pedesseau, C. Katan, M. Kepenekian, C. M. M. Soe, K. Appavoo, M. Y. Sfeir, S. Tretiak, P. M. Ajayan, M. G. Kanatzidis, J. Even, J. J. Crochet, A. D. Mohite, *Science* **2017**, 355, 1288.
- [30] S. Ahn, M. Park, S. Jeong, Y. Kim, J. Park, S. Kim, H. Kim, H. Cho, C. Wolf, M. Pei, H. Yang, T.-W. Lee, *Adv. Funct. Mater.* **2019**, 29, 1807535.
- [31] G. Xing, B. Wu, X. Wu, M. Li, B. Du, Q. Wei, J. Guo, E. K. L. Yeow, T. C. Sum, W. Huang, *Nat. Commun.* **2017**, 8, 14558.
- [32] M. Jang, M. Lee, H. Shin, J. Ahn, M. Pei, J. H. Youk, H. Yang, *Adv. Mater. Interfaces* **2016**, 3, 1600284.
- [33] J. C. de Mello, H. F. Wittmann, R. H. Friend, *Adv. Mater.* **1997**, 9, 230.